amcs

A ROBUST PATH FOLLOWING ALGORITHM BASED ON THE ORTHOGONAL BISHOP PARAMETRIZATION FOR A NON–HOLONOMIC MOBILE MANIPULATOR

ALICJA MAZUR [a], FILIP DYBA [a,*]

[a] Department of Cybernetics and Robotics
Wrocław University of Science and Technology
Janiszewskiego Street 11/17, 50-372 Wrocław, Poland
e-mail: {alicja.mazur,filip.dyba}@pwr.edu.pl

We deal with the fundamental problem of path following applied to control mobile manipulators. A parametric-based path following algorithm is proposed. Such an approach results in a cascaded structure of the control system, so that the control algorithm is designed using the backstepping integrator method. The proposed solution is robust due to the following features. Firstly, it is based on the Bishop parametrization, which is well-defined at every point of the curve. Moreover, we present a novel approach to the orthogonal projection method onto the path so that the motion precisely along the path is possible. Finally, the robustness to structural and parametric uncertainties of the dynamics model is guaranteed thanks to the sliding mode controller applied at the dynamic level of the control cascade. The problem is analyzed theoretically. The achieved results are verified with an exemplary simulation study. The proposed algorithm assures asymptotic convergence of errors to zero for less strict requirements imposed on the desired path and in the case of partial knowledge of the dynamics model.

Keywords: backstepping integrator control, non-holonomic mobile manipulator, orthogonal Bishop parametrization, singularity avoidance, path following algorithm, sliding mode controller.

1. Introduction

Over the past decades the control problem of robotic systems, especially with motion constraints, has attracted a great deal of attention. The importance of robotic solutions in industry is constantly growing as they allow improving precision in manufacturing processes and reduce production costs. The execution of a complex robot motion is usually performed as the trajectory tracking task, i.e., a motion with restricted time regime. In such a case robots are forced to achieve very high velocities: trajectories as "curves parametrized by time" have to be executed very fast. However, in many practical situations system velocities are bounded due to limited actuations. The solution to a required motion constrained with limited speed is the path following.

According to Hung *et al.* (2023), the path following task is controlling a robot position in order to reach and follow a spatial curve while a velocity profile along

the path is asymptotically tracked. The path is a pure geometrical object, often resulting from path planning algorithms, which have been eagerly developed by many researchers, for example by Pepy *et al.* (2009), Przybylski and Putz (2017), Jafarzadeh and Fleming (2018), Costa and Silva (2019) or Sun and Liu (2021).

There are different approaches to the path following problem. One may distinguish two main trends, namely parametric and non-parametric. Parametric solutions are often based on the formalism of curvilinear parametrizations which define a local frame evolving along the path according to its geometry. Robot behaviour is designed with respect to the particular non-inertial frame associated with the desired path. Such methods are eagerly considered in the literature and practical applications. They have been discussed for mobile robots (Liao *et al.*, 2015; Micaelli and Samson, 1993) and holonomic fixed-base manipulators on a plane (Galicki, 2006). These papers deal with two-dimensional cases, which are not easily scalable to

---

the three-dimensional space. Solutions in the 3D space have been presented for holonomic manipulators (Mazur *et al.*, 2015; Mazur and Dyba, 2023), autonomous underwater vehicles (Encarnação and Pascoal, 2000), and a group of robots (Cichella *et al.*, 2012). The path following task has been also studied for flying robots (Lugo-Cárdenas *et al.*, 2017), but the presented solution is restricted only to a kinematic analysis.

On the other hand, the non-parametric solutions are also investigated. This approach is mainly based on purely computational methods which frequently require defining the zero-level set, e.g., (Michałek and Gawron, 2018) or (Li *et al.*, 2020). Deriving a zero-level set is a non-trivial task. However, it can be used to consider speed limits or obstacles in the task (Gonçalves *et al.*, 2020). Vector fields have also been eagerly considered in non-parametric solutions, e.g., (Michałek and Kozłowski, 2009) or (Michałek and Gawron, 2018). A vector field is designed in such a way so that its integral curves converge to the desired path (Kapitanyuk *et al.*, 2018). Although methods based on vector fields have suitable representation, a certain effort has to be made to assure that method singularities are avoided.

The vector-field-based methods can also benefit from a parametric representation of a curve which can be defined by n scalar functions (Gonçalves *et al.*, 2010). Such an approach may result in a high dimensionality of the task (n-dimensional vector fields). The dimension may be even increased to avoid problems with singularities in the curve definition (Yao *et al.*, 2021). It results in higher problem complexity in comparison with methods based on curvilinear parametrization. On the other hand, vector fields seem suitable to deal with time-varying curves (Gonçalves *et al.*, 2010), but undesirable stable equilibrium points must be dealt with. Rezende *et al.* (2022) proposed a solution to that problem using a definition of the vector field based on elements of a curvilinear parametrization of the desired path. Rezende *et al.* (2022) indicated a problem with equidistant points to a curve. To solve the issue, they wondered about including the minimum distance from a curve in the state of a vector field and defining a propagation law for this parameter. In fact, such an approach is a fundamental aspect of methods based on curvilinear parametrization.

In this paper, we focus on a method based on the curvilinear parametrization formalism. Although this approach is not free from drawbacks, it has a nice geometric interpretation and results in low dimensionality of the task. In fact, the task dimensionality directly corresponds to the dimensions of a robot workspace. The most popular curvilinear parametrization method considered in the path following task was proposed by Serret (1851) and Frenet (1852). However, it is indeterminate when the path curvature is null. An alternative method was introduced by Bishop (1975).

The usage of the Bishop parametrization leads to a significant improvement in the generalization of the robot description with respect to the given path.

Furthermore, in order to obtain equations of motion with respect to the reference path described by a curvilinear parametrization, a virtual target on the path is considered. It can be located at any distance from the controlled robot, which results in a non-orthogonal parametrization (Mazur and Dyba, 2023). Alternatively, a controlled robot can be located always at the shortest distance from a target to obtain the orthogonal projection of the robot onto the path (Mazur *et al.*, 2015). In the second approach, the problem dimensionality is minimised thanks to the assumption of the closest proximity between the robot and the path. On the other hand, it introduces a singularity to the robot description. Thus, the parametrization is defined locally, near the path.

The parametric-based approach to the path following problem results in a certain structure of the control system. The mathematical model of a robot for the path following task includes the robot dynamics as a set of second-order differential equations, and the robot kinematics as a set of the first-order differential equations (description of the end-effector motion relative to the local frame associated with the path). The equations describing the kinematic and dynamic behaviour of the plant are coupled and can be described as a two-stage cascade system. Such a cascade structure has been eagerly used for control purposes, for instance by Soetanto *et al.* (2003) or Kozłowski and Pazderski (2004). In such a control structure there exist subsystems that cannot be controlled via the external inputs. However, they are commanded due to appropriate control design on the respective cascade levels. According to Krstić *et al.* (1995), the backstepping integrator algorithm can be used as an efficient control method for the cascaded systems.

In this article, we also focus on a particular type of robots, namely mobile manipulators. They are willingly included in the research and applications as they are particularly relevant to the automation of freight transport and complex lifting operations. A mobile manipulator is described as a robotic system composed of two separate subsystems: a mobile platform and an on-board manipulator. Taking into account the mobility of the subsystems, i.e., the type of constraints occurring in motion, there are four possible configurations of mobile manipulators. They concern holonomic properties either of the platform or the manipulator. The most popular is the combination (nh, h), i.e., a non-holonomic base and a holonomic manipulator. Such a system can perform manipulation tasks in a larger workspace than a fixed-base manipulator. The price that should be paid for such an advantage is a more complex modelling description and control design (Mazur, 2010), which are considered within this article.

The control problem of mobile manipulators has already been addressed in the literature, e.g. by Mazur (2004) or Mazur and Szakiel (2009), where the path following problem was considered. The authors provided solutions for mobile manipulators of type (nh, h) and (nh, nh). However, they treated the path following task for every subsystem separately and based their control strategies on the Serret–Frenet parametrization.

The contribution of our paper is the following:

- A new control algorithm for non-holonomic mobile manipulators of the type (nh, h) is presented. The aim of the algorithm is to allow the manipulator end-effector to follow 3D paths defined by curves of at least class $\mathcal{C}^2$, without dividing the task into the separate subtasks for the platform and the robotic arm.

- The robot description with respect to the given path is achieved by using the orthogonal Bishop parametrization. This is a generalization of the previously considered methods as it has no indeterminacy points resulting from the curve geometry. A novel approach to the formulation of the orthogonal projection constraint is also discussed. It allows us to avoid or translate the singularity of the method. As a result, the end-effector is able to move precisely along the path, not only to asymptotically approach it.

- The proposed control law is robust to structural or parametric uncertainties of the robot dynamics. The algorithm is designed with the backstepping integrator method. On the first level (the kinematics level) velocity profiles are generated in order to follow the path and stick to the motion constraints resulting from the platform non-holonomy. On the dynamics level a sliding mode controller (Slotine and Li, 1991; Utkin, 1992) is harnessed. The sliding mode controllers have already been considered in many applications, for instance, by Bartoszewicz and Adamiak (2019), or Abadi *et al.* (2020). We tailor this method to the path following problem and the specificity of mobile manipulators. The formal analysis is provided to show that the algorithm guarantees asymptotic convergence of errors to zero despite the dynamics uncertainty. The theoretical stability of the algorithm is verified with a simulation study.

2. Mathematical description of the robot

The considered robot is a mobile manipulator of the type (nh, h) that consists of a non-holonomic mobile platform equipped with non-deformable wheels and a holonomic rigid manipulator mounted on its top. The state of the mobile manipulator is described as

$$\boldsymbol{q} = \begin{pmatrix} \boldsymbol{q}_m \\ \boldsymbol{q}_r \end{pmatrix}, \tag{1}$$

where $\boldsymbol{q}_m \in \mathbb{R}^n$ is the platform state and $\boldsymbol{q}_r \in \mathbb{R}^p$ is the vector of joint positions.

It is assumed that non-holonomic constraints are imposed on the mobile platform. In the system there are no longitudinal slippage for every wheel and no lateral slippage (Spong and Vidyasagar, 1991). Such constraints may be expressed in the Pfaffian form

$$\boldsymbol{A}(\boldsymbol{q}_m)\dot{\boldsymbol{q}}_m = \boldsymbol{0}, \tag{2}$$

with $\boldsymbol{A}(\boldsymbol{q}_m) \in \mathbb{R}^{l \times n}$, where l is a number of independent constraints. Non-holonomic constraints can be expressed also as a driftless control system

$$\dot{\boldsymbol{q}}_m = \boldsymbol{G}(\boldsymbol{q}_m)\boldsymbol{\eta}, \tag{3}$$

where the matrix $\boldsymbol{G}(\boldsymbol{q}_m) \in \mathbb{R}^{n \times m}$, $m = n - l$, and the vector $\boldsymbol{\eta} \in \mathbb{R}^m$ defines the so-called auxiliary velocities (Campion *et al.*, 1996). The matrix $\boldsymbol{G}(\boldsymbol{q}_m)$ is chosen in order to span the kernel of the Pfaffian matrix $\boldsymbol{A}(\boldsymbol{q}_m)$, i.e., that $\boldsymbol{A} \cdot \boldsymbol{G} \equiv \boldsymbol{0}$ holds.

The position and orientation of the end-effector in the inertial frame $X_0 Y_0 Z_0$ are described by the expression

$$\boldsymbol{p}(\boldsymbol{q}) = \boldsymbol{p}(\boldsymbol{q}_m, \boldsymbol{q}_r) \in \mathbb{R}^k. \tag{4}$$

Hence, the end-effector velocity may be expressed as

$$\dot{\boldsymbol{p}} = \frac{\partial \boldsymbol{p}}{\partial \boldsymbol{q}}\dot{\boldsymbol{q}} = \left[\frac{\partial \boldsymbol{p}}{\partial \boldsymbol{q}_m} \ \frac{\partial \boldsymbol{p}}{\partial \boldsymbol{q}_r} \right] \begin{pmatrix} \dot{\boldsymbol{q}}_m \\ \dot{\boldsymbol{q}}_r \end{pmatrix}$$
$$= \begin{bmatrix} \boldsymbol{J}_m & \boldsymbol{J}_r \end{bmatrix} \begin{pmatrix} \dot{\boldsymbol{q}}_m \\ \dot{\boldsymbol{q}}_r \end{pmatrix}.$$

It leads to the equation

$$\begin{aligned} \dot{\boldsymbol{p}} &= \begin{bmatrix} \boldsymbol{J}_m & | & \boldsymbol{J}_r \end{bmatrix} \begin{pmatrix} \dot{\boldsymbol{q}}_m \\ \dot{\boldsymbol{q}}_r \end{pmatrix} \\ &= \begin{bmatrix} \boldsymbol{J}_m & | & \boldsymbol{J}_r \end{bmatrix} \begin{pmatrix} \boldsymbol{G}\boldsymbol{\eta} \\ \dot{\boldsymbol{q}}_r \end{pmatrix} \\ &= \begin{bmatrix} \boldsymbol{J}_m\boldsymbol{G} & | & \boldsymbol{J}_r \end{bmatrix} \begin{pmatrix} \boldsymbol{\eta} \\ \dot{\boldsymbol{q}}_r \end{pmatrix} \\ &= \begin{bmatrix} \boldsymbol{J}_m^* & | & \boldsymbol{J}_r \end{bmatrix} \boldsymbol{z} \\ &= \boldsymbol{J}^*(\boldsymbol{q})\boldsymbol{z}, \end{aligned} \tag{5}$$

where $\boldsymbol{z} = \begin{pmatrix} \boldsymbol{\eta}^T & \dot{\boldsymbol{q}}_r^T \end{pmatrix}^T$ is the vector of auxiliary velocities for the (nh, h) mobile manipulator and $\boldsymbol{J}^* \in \mathbb{R}^{k \times (m+p)}$ is the Jacobi matrix describing the relationship between velocities of the mobile manipulator end-effector $\dot{\boldsymbol{p}}$ and auxiliary velocities $\boldsymbol{z}$. In Eqn. (5) the non-holonomic constraints of the mobile platform are taken into account by introducing the matrix $\boldsymbol{G}(\boldsymbol{q}_m)$.

Dynamics of the system may be derived using the d'Alembert principle (Mazur, 2004). It is expressed with the equation (Mazur and Płaskonka, 2012)

$$Q(q)\ddot{q} + C(\dot{q}, q)\dot{q} + D(q) = \begin{bmatrix} A^T \\ 0 \end{bmatrix} \lambda + B\tau, \quad (6)$$

where the following elements are defined:

- $Q(q) = \begin{bmatrix} Q_{11} & Q_{12} \\ Q_{21} & Q_{22} \end{bmatrix} \in \mathbb{R}^{(n+p)\times(n+p)}$ is the inertia matrix of the mobile manipulator;

- $C(q, \dot{q}) = \begin{bmatrix} C_{11} & C_{12} \\ C_{21} & C_{22} \end{bmatrix} \in \mathbb{R}^{(n+p)\times(n+p)}$ is the matrix of Coriolis and centrifugal forces acting on the mobile manipulator;

- $D(q) = \begin{pmatrix} 0 \\ D_2 \end{pmatrix} \in \mathbb{R}^{n+p}$ is the gravity vector; it is assumed that the mobile platform moves only on the $X_0 Y_0$ plane;

- $\lambda \in \mathbb{R}^l$ is the vector of Lagrange multipliers, which have a sense of static friction forces; non-holonomic constraints are defined only for the mobile platform;

- $B = \begin{bmatrix} B_m & 0 \\ 0 & I_p \end{bmatrix} \in \mathbb{R}^{(n+p)\times(m+p)}$ is the input matrix;

- $\tau = \begin{pmatrix} \tau_m \\ \tau_r \end{pmatrix} \in \mathbb{R}^{m+p}$ is the control vector; the vector τ_m represents control torques in the platform wheels, while τ_r stands for control generalized forces in the manipulator joints.

Let us observe that the elements Q_{12}, Q_{21}, C_{12} and C_{21} result from the dynamic coupling between the mobile platform and the manipulator.

Subsequently, the dynamics is expressed with the auxiliary coordinates z. It is derived by pre-multiplying Eqn. (6) by the matrix $\begin{bmatrix} G^T & 0 \\ 0 & I_p \end{bmatrix}$. Considering also the driftless system, Eqn. (3), and its time derivative, the dynamics model is expressed as

$$Q^*(q)\dot{z} + C^*(q, \dot{q})z + D^*(q) = B^*(q)\tau, \quad (7)$$

where $Q^*(q), C^*(q, \dot{q}), B^*(q) \in \mathbb{R}^{(m+p)\times(m+p)}$ and

$$Q^*(q) = \begin{bmatrix} G^T Q_{11} G & G^T Q_{12} \\ Q_{21} G & Q_{22} \end{bmatrix},$$

$$C^*(q, \dot{q}) = \begin{bmatrix} G^T C_{11} G + G^T Q_{11} \dot{G} & G^T C_{12} \\ C_{21} G + Q_{21} \dot{G} & C_{22} \end{bmatrix},$$

$$D^*(q) = \begin{pmatrix} 0 \\ D_2 \end{pmatrix} \in \mathbb{R}^{m+p},$$

$$B^*(q) = \begin{bmatrix} G^T B & 0 \\ 0 & I_p \end{bmatrix}.$$

Property 1. (*Skew-symmetry of the inertia matrix*) According to Dulęba (2000), the inertia matrix Q^* of a mobile manipulator does not preserve the property of skew-symmetry, which is typical for fixed-base manipulators. Therefore, a correction matrix C^γ is defined to satisfy the following relation:

$$\dot{Q}^* = (C^* + C^\gamma) + (C^* + C^\gamma)^T. \quad (8)$$

3. Bishop parametrization

The Bishop parametrization (Bishop, 1975) allows one to define a local frame associated with a curve. The evolution of the frame along the curve is strictly defined by its geometry. It is an alternative parametrization method to the one presented simultaneously by Serret (1851) and Frenet (1852). Comparing both the methods, it can be observed that the Bishop frame offers clear advantages over the Serret–Frenet parametrization. The Bishop frame

- is well defined at all zero-curvature points (Carroll *et al.*, 2013) in contrast to the Serret–Frenet frame;

- can be used to parametrize paths with zero curvature; in particular, it enables to derive parametrization of a straight line, which is a common motion component;

- evolves continuously along a curve due to the lack of indeterminacy points (Carroll *et al.*, 2013);

- reduces the requirement on the minimal curve class to $\mathcal{C}^2$ (for the Serret–Frenet method a curve has to be at least class $\mathcal{C}^3$);

- expands the scope of curves which may be considered as the desired path in the path following task;

- minimizes the frame rotations along the curve (Selig and Wu, 2006);

- can be rotated in the initial state, although its evolution remains unique.

The Bishop frame consists of a vector tangent to a curve r, denoted as T, and two of its normal vectors. If the curve is expressed with respect to the arc length, s, called also as curvilinear distance (Oprea, 1997), the tangent vector is defined as

$$T(s) = \frac{\mathrm{d}r(s)}{\mathrm{d}s}. \quad (9)$$

The normal vectors $\{N_1, N_2\}$ are chosen in such a way as to create with the tangential vector an orthonormal basis in $\mathbb{R}^3$. The evolution of the normal vectors is defined with

the relatively parallel transport (Bishop, 1975; Lee, 1997). This means that the following relation holds:

$$\frac{\mathrm{d}\boldsymbol{N}_i(s)}{\mathrm{d}s} = g_i(s)\boldsymbol{T}(s), \quad i \in \{1, 2\}, \qquad (10)$$

where $g_i(s)$ are functions defined by some geometric invariants of the Bishop parametrization, $k_1(s)$ and $k_2(s)$, resulting from the curve geometry. They do not have an intuitive interpretation like curvature or torsion, but explicitly depend on them (Bishop, 1975). Hence, the evolution of the Bishop frame may be described as

$$\frac{\mathrm{d}\boldsymbol{T}(s)}{\mathrm{d}s} = k_1(s)\boldsymbol{N}_1(s) + k_2(s)\boldsymbol{N}_2(s), \qquad (11a)$$

$$\frac{\mathrm{d}\boldsymbol{N}_1(s)}{\mathrm{d}s} = -k_1(s)\boldsymbol{T}(s), \qquad (11b)$$

$$\frac{\mathrm{d}\boldsymbol{N}_2(s)}{\mathrm{d}s} = -k_2(s)\boldsymbol{T}(s). \qquad (11c)$$

These equations may be expressed in the matrix form

$$\begin{aligned}\frac{\mathrm{d}\boldsymbol{S}(s)}{\mathrm{d}s} &= \begin{bmatrix} \dfrac{\mathrm{d}\boldsymbol{T}(s)}{\mathrm{d}s} & \dfrac{\mathrm{d}\boldsymbol{N}_1(s)}{\mathrm{d}s} & \dfrac{\mathrm{d}\boldsymbol{N}_2(s)}{\mathrm{d}s} \end{bmatrix} \\ &= \begin{bmatrix} \boldsymbol{T}^T(s) \\ \boldsymbol{N}_1^T(s) \\ \boldsymbol{N}_2^T(s) \end{bmatrix}^T \begin{bmatrix} 0 & -k_1(s) & -k_2(s) \\ k_1(s) & 0 & 0 \\ k_2(s) & 0 & 0 \end{bmatrix} \\ &= \boldsymbol{S}(s)\boldsymbol{W}(s). \end{aligned}$$
$$(12)$$

The matrix $\boldsymbol{S}(s) \in \mathbb{SO}(3)$ describes the orientation of the Bishop frame with respect to the inertial frame. The matrix $\boldsymbol{W}(s)$ is a skew-symmetric matrix by construction and its elements are the Bishop geometric invariants. The evolution of the matrix $\boldsymbol{S}(s)$ in the time domain is defined with the following equation:

$$\dot{\boldsymbol{S}}(s) = \frac{\mathrm{d}\boldsymbol{S}(s)}{\mathrm{d}s}\dot{s} = \dot{s}\boldsymbol{S}(s)\boldsymbol{W}(s). \qquad (13)$$

The pair (k_1, k_2) is called the normal development of the curve (Bishop, 1975). It may be calculated based on Eqns. (11), and the assumption that the base vectors are orthonormal (Liu and Pei, 2013),

$$k_1(s) = \left\langle \frac{\mathrm{d}\boldsymbol{T}(s)}{\mathrm{d}s}, \boldsymbol{N}_1(s) \right\rangle, \qquad (14a)$$

$$k_2(s) = \left\langle \frac{\mathrm{d}\boldsymbol{T}(s)}{\mathrm{d}s}, \boldsymbol{N}_2(s) \right\rangle, \qquad (14b)$$

where $\langle \cdot, \cdot \rangle$ denotes the scalar product of vectors. The values defined in Eqns. (14a) and (14b) are necessary for computing the Bishop frame evolution.

The presented Bishop parametrization equations can be harnessed to describe the robot state with respect to a given curve.
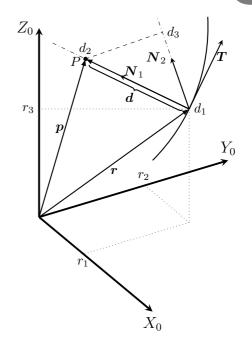

Fig. 1. Orthogonal projection of an object onto a curve.

4. Robot equations with respect to the Bishop frame avoiding singularity

In order to enforce the robot to move along the path, we describe the end-effector position with respect to the local frame associated with the given path via the Bishop parametrization method. As a consequence, the description of the controlled object with respect to the moving frame is derived. This motion is fully defined with the path geometry, so if the robot mimics it, the path following problem is solved.

It is assumed that the end-effector position in the inertial frame $\boldsymbol{p}$ is projected orthogonally onto the curve parametrized with the Bishop frame. As a result, the end-effector is always located at the point of the closest distance to the curve, i.e., in the plane spanned by the normal vectors, $\boldsymbol{N}_1$ and $\boldsymbol{N}_2$. A schematic view of the orthogonal projection is presented in Fig. 1. Define the position of the manipulator end-effector in the Bishop frame as

$$\boldsymbol{d} = \begin{pmatrix} d_1 & d_2 & d_3 \end{pmatrix}^T = \boldsymbol{S}^T(\boldsymbol{p} - \boldsymbol{r}). \qquad (15)$$

According to the assumption of the orthogonal projection, the distance in the tangent direction d_1 should always be zero. This implies that the vectors $(\boldsymbol{p} - \boldsymbol{r})$ and $\boldsymbol{T}$ are orthogonal, i.e.,

$$\langle \boldsymbol{T}, \boldsymbol{p} - \boldsymbol{r} \rangle = 0. \qquad (16)$$

The time derivative of Eqn. (16) is

$$\left\langle \frac{\mathrm{d}\boldsymbol{T}}{\mathrm{d}s}\dot{s}, \boldsymbol{p} - \boldsymbol{r} \right\rangle + \langle \boldsymbol{T}, \dot{\boldsymbol{p}} - \dot{\boldsymbol{r}} \rangle = 0. \qquad (17)$$

Considering the relation

$$\langle \boldsymbol{T}, \dot{\boldsymbol{r}} \rangle = \left\langle \boldsymbol{T}, \frac{\mathrm{d}\boldsymbol{r}}{\mathrm{d}s}\dot{s} \right\rangle = \dot{s}\langle \boldsymbol{T}, \boldsymbol{T} \rangle = \dot{s}, \qquad (18)$$

the condition which guarantees the fulfilment of the orthogonal projection assumption is derived based on Eqn. (17),

$$\dot{s} = -\frac{\langle \boldsymbol{T}, \dot{\boldsymbol{p}} \rangle}{\langle \frac{\mathrm{d}\boldsymbol{T}}{\mathrm{d}s}, \boldsymbol{p} - \boldsymbol{r} \rangle - 1}. \qquad (19)$$

Taking into account Eqns. (11a) and (15), Eqn. (19) can be reformulated as

$$\dot{s} = -\frac{\langle \boldsymbol{T}, \dot{\boldsymbol{p}} \rangle}{k_1 d_2 + k_2 d_3 - 1}. \qquad (20)$$

It is noteworthy that the singularity defined in Eqn. (19) is shifted in comparison with the previous form of the orthogonal projection constraint used, e.g., by Mazur *et al.* (2015). In the new approach, the expression $\langle \frac{\mathrm{d}\boldsymbol{T}}{\mathrm{d}s}, \boldsymbol{p} - \boldsymbol{r} \rangle = k_1 d_2 + k_2 d_3$ may be null and Eqns. (19), (20) are still well defined. Although the new definition of the orthogonal projection constraint remains local as $k_1 d_2 + k_2 d_3 \neq 1$, it allows us to fully benefit from the Bishop parametrization method. The manipulator end-effector can be located precisely on the given curve and move along zero-curvature paths, when $(k_1, k_2) = (0, 0)$. The main drawbacks resulting from the singularity of the orthogonal projection constraint have been overcome by translating the singularity to another point outside the reference path (Dyba and Mazur, 2024).

Consider now the evolution of the end-effector position with respect to the Bishop frame. It is described by the derivative of Eqn. (15)

$$\dot{\boldsymbol{d}} = \boldsymbol{S}^T(\dot{\boldsymbol{p}} - \dot{\boldsymbol{r}}) + \dot{\boldsymbol{S}}^T(\boldsymbol{p} - \boldsymbol{r}). \qquad (21)$$

Equation (21) may be rewritten as

$$\dot{d}_1 = \langle \boldsymbol{T}, \dot{\boldsymbol{p}} - \dot{\boldsymbol{r}} \rangle + \dot{s}k_1\langle \boldsymbol{N}_1, \boldsymbol{p} - \boldsymbol{r} \rangle$$
$$+ \dot{s}k_2\langle \boldsymbol{N}_2, \boldsymbol{p} - \boldsymbol{r} \rangle, \qquad (22a)$$
$$\dot{d}_2 = \langle \boldsymbol{N}_1, \dot{\boldsymbol{p}} - \dot{\boldsymbol{r}} \rangle - \dot{s}k_1\langle \boldsymbol{T}, \boldsymbol{p} - \boldsymbol{r} \rangle$$
$$= \langle \boldsymbol{N}_1, \dot{\boldsymbol{p}} - \dot{\boldsymbol{r}} \rangle, \qquad (22b)$$
$$\dot{d}_3 = \langle \boldsymbol{N}_2, \dot{\boldsymbol{p}} - \dot{\boldsymbol{r}} \rangle - \dot{s}k_2\langle \boldsymbol{T}, \boldsymbol{p} - \boldsymbol{r} \rangle$$
$$= \langle \boldsymbol{N}_2, \dot{\boldsymbol{p}} - \dot{\boldsymbol{r}} \rangle. \qquad (22c)$$

After a short computation involving Eqns. (18) and (20), it can be shown that Eqn. (22a) confirms maintaining a constant distance in the tangent vector direction as $\dot{d}_1 = 0$. As a result, the orthogonal projection assumption is satisfied. Due to that fact, we need to assure the satisfaction of the orthogonal projection constraint by controlling the variable s. Apart from that, it is still necessary to control the end-effector position in the

normal vectors directions. As a consequence, the state of the end-effector with respect to the local Bishop frame can be expressed with the following variables:

$$\boldsymbol{\xi} = \begin{pmatrix} s & d_2 & d_3 \end{pmatrix}^T. \qquad (23)$$

The vector $\boldsymbol{\xi}$ reduces the dimensionality of the path following problem as the position in the tangent vector direction is not taken into account. The time derivatives of the vector $\boldsymbol{\xi}$ elements are defined as

$$\dot{s} = -\frac{\boldsymbol{T}^T}{k_1 d_2 + k_2 d_3 - 1}\dot{\boldsymbol{p}} = \boldsymbol{f}_1\dot{\boldsymbol{p}}, \qquad (24a)$$
$$\dot{d}_2 = \boldsymbol{N}_1^T\dot{\boldsymbol{p}} - \langle \boldsymbol{N}_1, \dot{\boldsymbol{r}} \rangle$$
$$= \boldsymbol{N}_1^T\dot{\boldsymbol{p}} - \left\langle \boldsymbol{N}_1, \frac{\mathrm{d}\boldsymbol{r}}{\mathrm{d}s}\dot{s} \right\rangle$$
$$= \boldsymbol{N}_1^T\dot{\boldsymbol{p}} - \dot{s}\langle \boldsymbol{N}_1, \boldsymbol{T} \rangle$$
$$= \boldsymbol{N}_1^T\dot{\boldsymbol{p}} = \boldsymbol{f}_2\dot{\boldsymbol{p}}, \qquad (24b)$$
$$\dot{d}_3 = \boldsymbol{N}_2^T\dot{\boldsymbol{p}} - \langle \boldsymbol{N}_2, \dot{\boldsymbol{r}} \rangle$$
$$= \boldsymbol{N}_2^T\dot{\boldsymbol{p}} - \left\langle \boldsymbol{N}_2, \frac{\mathrm{d}\boldsymbol{r}}{\mathrm{d}s}\dot{s} \right\rangle$$
$$= \boldsymbol{N}_2^T\dot{\boldsymbol{p}} - \dot{s}\langle \boldsymbol{N}_2, \boldsymbol{T} \rangle$$
$$= \boldsymbol{N}_2^T\dot{\boldsymbol{p}} = \boldsymbol{f}_3\dot{\boldsymbol{p}}. \qquad (24c)$$

Equations (24) may be also rewritten in the concise form

$$\dot{\boldsymbol{\xi}} = \boldsymbol{F}\dot{\boldsymbol{p}}, \qquad (25)$$

where $\boldsymbol{F} = \begin{bmatrix} \boldsymbol{f}_1^T & \boldsymbol{f}_2^T & \boldsymbol{f}_3^T \end{bmatrix}^T$. Equation (25) fully defines the evolution of the end-effector in the local Bishop frame associated with a certain curve.

5. Control law formulation

The control problem considered in the article is following a desired path of at least class $\mathcal{C}^2$ located in the robot workspace by a non-holonomic mobile manipulator. Only control of the position with respect to the given curve is taken into account.

It is assumed that the orthogonal Bishop parametrization is used to derive robot equations with respect to the path. It may be noticed that Eqn. (25), which describes the end-effector motion dynamics with respect to the curve, has a similar form to the first-order non-holonomic constraints (velocity constraints). It means that the control problem is defined by

- the plant dynamics, Eqn. (7),

- the non-holonomic constraints of the robot platform, Eqn. (3),

- the description of robot motion relative to the given path in $\mathbb{R}^3$, Eqn. (25).
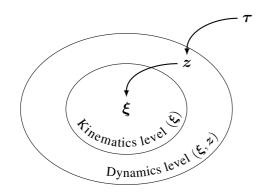
Fig. 2. Cascaded structure of the mobile manipulator system.

It is noteworthy that apart from the non-holonomic constraints there are additional kinematic constraints in the system which impose the successful following of the path. In fact, the constraints, Eqns. (3) and (25), are connected via Eqn. (5). Thus, the equation including all kinematic constraints takes the form

$$\dot{\boldsymbol{\xi}} = \boldsymbol{F}\dot{\boldsymbol{p}} = \boldsymbol{F}\boldsymbol{J}^{*}\boldsymbol{z} = \boldsymbol{L}\boldsymbol{z}, \qquad (26)$$

where $\boldsymbol{L} = \boldsymbol{F}\boldsymbol{J}^{*} \in \mathbb{R}^{3\times(m+p)}$ is a full row rank matrix.

The variable $\boldsymbol{\xi}$ is the state variable on the kinematics level. It can be controlled via the auxiliary velocity $\boldsymbol{z}$, which is the state variable on the dynamics level. According to Eqn. (7), it can be controlled using the external input $\boldsymbol{\tau}$. Hence, the kinematic constraints (26) are coupled with the robot dynamics, Eqn. (7), and the equations form a two-stage cascaded system which is presented in Fig. 2.

The backstepping integrator algorithm (Krstić *et al.*, 1995) may be used for the design of the control law as the general methodology for the cascaded systems. It allows us to derive equations of constraints on the system trajectories at every cascade level and take them into account at higher stages. As a result, the external control input is designed so that it satisfies all the constraints of the system. In the considered case it is necessary to design two controllers (each for every stage) working simultaneously:

1. Kinematic controller (constraints (26) are considered): On the first stage of the cascade, i.e., the kinematics level, velocity profiles $\boldsymbol{z}_{\text{ref}}$ should be generated in order to fulfil constraints resulting from the given path and the non-holonomy of the mobile platform. However, the reference velocities cannot be commanded directly as they are a part of the system trajectories. In fact, the kinematic controller determines geometrically the desired trajectory in the state variables space, so it performs as a *motion planner*.

2. Dynamic controller: The velocity profiles generated

by the kinematic controller have to be enforced by a control law on the second stage of the cascade, i.e., at the dynamics level. That is, control torques and forces $\boldsymbol{\tau}$ are generated based on the calculated velocity profiles. The dynamic controller is responsible for controlling the generalized forces in order to follow the trajectory in the state space, so it can be treated as a *motion executor*.

The schematic view of the control structure is presented in Fig. 3.

In the proposed cascade structure subsystems influence each other, but the control signals are applied only to the most outer one. Hence, we must assure that the function forms of errors at the higher cascade stage are defined by trajectories describing error dynamics at the lower level. Therefore, according to Krstić *et al.* (1995), the control design should start from the innermost subsystem as though no higher stage existed. On every higher level the formulated control laws have to be taken into account.

Remark 1. It is noteworthy that the velocities $\boldsymbol{z}$ are parts of the system trajectories and state variables on the dynamics level. Hence, they are controlled only indirectly. However, the velocity profiles, $\boldsymbol{z}_{\text{ref}}$, are treated as control inputs on the kinematics level for the design purposes. The velocity profiles are used to close a control loop on the kinematics level. In practice, the kinematic controller is responsible only for planning velocity profiles to satisfy kinematic constraints. It is the dynamic controller which forces the system trajectories, $\boldsymbol{z}$, to converge to the planned velocity profiles, $\boldsymbol{z}_{\text{ref}}$.

6. Main result: Control algorithm

6.1. Kinematic controller. As mentioned, the kinematic constraints for the considered system are given by Eqn. (26). Based on that equation the following kinematic controller is proposed:

$$\boldsymbol{z}_{\text{ref}} = \boldsymbol{L}^{\#}\left(\dot{\boldsymbol{\xi}}_{d} - \boldsymbol{K}_{k}\boldsymbol{e}_{\boldsymbol{\xi}}\right), \qquad (27)$$

where $\boldsymbol{\xi}_{d} = \boldsymbol{\xi}_{d}(t)$ is the desired state of a robot with respect to the local Bishop frame associated with the desired path, $\boldsymbol{e}_{\boldsymbol{\xi}} = \boldsymbol{\xi} - \boldsymbol{\xi}_{d}$ is the vector of path following errors, $\boldsymbol{K}_{k} = \text{diag}\{k_{k}\}$ is the positive-definite gain matrix, $k_{k} > 0$, and $\#$ denotes the Moore-Penrose pseudoinverse of a matrix (Spong and Vidyasagar, 1991), i.e.,

$$\boldsymbol{L}^{\#} = \boldsymbol{L}^{T}(\boldsymbol{L}\boldsymbol{L}^{T})^{-1}.$$

It is assumed that the robot operates outside singular configurations. Thus, the matrix $\boldsymbol{L}$ is full row rank and its pseudo-inverse $\boldsymbol{L}^{\#}$ is well defined. It is stated that the proposed control law allows following the desired path according to the following result:
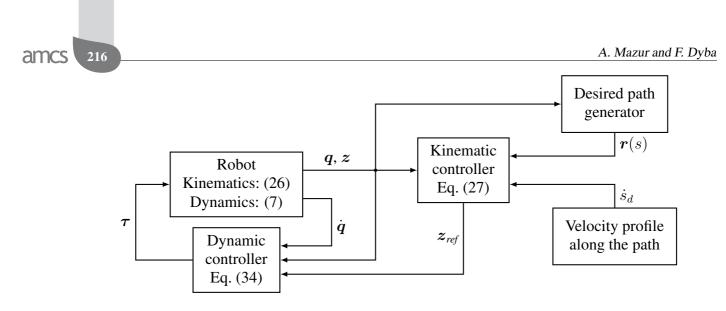
Fig. 3. General scheme of the cascade control structure.

Theorem 1. *The reference velocity profiles* (27) *guarantee the asymptotic convergence of the path following errors,* e_ξ *to zero.*

Proof. (Kinematic control law) In order to satisfy the kinematic constraints, the trajectories of the system (26), z, should converge to appropriate reference trajectories z_{ref}. According to the backstepping integrator method (Krstić *et al.*, 1995), the kinematic controller (27) is treated as a control command for the system (26) as though there were no higher levels of the control cascade. According to Remark 1, the velocity profiles (27), z_{ref}, constitute velocity controls for the system (26) to control the state ξ. As a result, the system (26) in the closed feedback loop with the control (27) is described by

$$\dot{e}_\xi + K_k e_\xi = 0. \tag{28}$$

The Lyapunov-like candidate function for the system (28) is defined as

$$V_1(e_\xi) = \frac{1}{2} e_\xi^T e_\xi. \tag{29}$$

Its time derivative calculated along trajectories of the system (28) is

$$\begin{aligned}
\dot{V}_1(e_\xi) &= e_\xi^T \dot{e}_\xi \\
&= e_\xi^T(-K_k e_\xi) \\
&= -e_\xi^T K_k e_\xi \\
&\leq -K_k \|e_\xi\|^2 = -W_1(e_\xi) \leq 0. \tag{30}
\end{aligned}$$

We have shown that the system (28) has a positive-definite Lyapunov-like function (29), and $\dot{V}_1(e_\xi) \leq 0$ for any $e_\xi \in \Upsilon^0 = \{e_\xi : V_1(e_\xi) < v_0\}$, where $v_0 > 0$. Hence, by virtue of the LaSalle invariance principle (Canudas de Wit *et al.*, 1996), all bounded solutions starting in Υ^0 tend to the maximum invariant

set Ω^0, which is an attracting set and a subset of the invariant set $\Omega = \{e_\xi \in \Upsilon^0 : \dot{V}_1(e_\xi) = 0\}$. Since

$$\dot{V}_1(e_\xi) = 0 \iff W_1(e_\xi) = K_k \|e_\xi\|^2 = 0,$$

the invariant set Ω is defined only by a single point $e_\xi = 0$ which is the equilibrium point of the system (28). Therefore, the maximum invariant set Ω_0 has to be equal to the invariant set Ω according to the relation

$$\Omega^0 = \Omega = \{e_\xi \in \Upsilon^0 : \|e_\xi\| = 0\}.$$

This means that the path following errors converge asymptotically to zero and the system (28) is asymptotically stable with a zero equilibrium point for any positive-definite matrix K_k. It guarantees that the designed reference velocities, z_{ref}, allow following the path correctly on the kinematics level. ∎

6.2. Dynamic controller. The second stage of the cascaded structure requires a dynamic controller which guarantees that the errors of following the velocity profiles generated by the kinematic controller converge to zero.

The errors considered on this stage of the cascade are the velocity profiles following errors defined as

$$e_z = z - z_{\text{ref}}, \tag{31}$$

where the reference velocity z_{ref} is defined by the output of the kinematic controller given by Eqn. (27). Hence, Eqn. (31) may be rewritten as

$$e_z(e_\xi) = z - L^\# \left(\dot{\xi}_d - K_k e_\xi \right). \tag{32}$$

Equation (32) shows that the errors defined for both the levels of the system are coupled. In particular, the function form of the velocity profiles following errors e_z is not

random, but is directly dependent on the path following errors e_ξ.

A sliding mode controller (Slotine and Li, 1991; Utkin, 1992) is proposed as a dynamic control law. This controller might be used when the structure of robot dynamics model or some model parameters are not known. It is robust to unknown external disturbances which are not taken into account in the dynamics model.

If the dynamics model linearly depends on the unknown parameters ρ and there are some structurally unknown parts $\zeta(t)$, Eqn. (7) is transformed to the form

$$
\begin{aligned}
\boldsymbol{Q}_k^*(\boldsymbol{q}, \boldsymbol{\rho})&\dot{\boldsymbol{z}} + \boldsymbol{C}_k^*(\boldsymbol{q}, \dot{\boldsymbol{q}}, \boldsymbol{\rho})\boldsymbol{z} + \boldsymbol{D}_k^*(\boldsymbol{q}, \boldsymbol{\rho}) + \boldsymbol{\zeta}(t) \\
&= \boldsymbol{Q}_0^*(\boldsymbol{q})\dot{\boldsymbol{z}} + \boldsymbol{C}_0^*(\boldsymbol{q}, \dot{\boldsymbol{q}})\boldsymbol{z} + \boldsymbol{D}_0^*(\boldsymbol{q}) \\
&\quad + \boldsymbol{Q}_{\boldsymbol{\rho}}^*(\boldsymbol{q})\dot{\boldsymbol{z}} + \boldsymbol{C}_{\boldsymbol{\rho}}^*(\boldsymbol{q}, \dot{\boldsymbol{q}})\boldsymbol{z} + \boldsymbol{D}_{\boldsymbol{\rho}}^*(\boldsymbol{q}) + \boldsymbol{\zeta}(t) \\
&= \boldsymbol{Q}_0^*(\boldsymbol{q})\dot{\boldsymbol{z}} + \boldsymbol{C}_0^*(\boldsymbol{q}, \dot{\boldsymbol{q}})\boldsymbol{z} + \boldsymbol{D}_0^*(\boldsymbol{q}) \\
&\quad + \boldsymbol{Y}(\dot{\boldsymbol{z}}, \boldsymbol{z}, \dot{\boldsymbol{q}}, \boldsymbol{q})\boldsymbol{\rho} + \boldsymbol{\zeta}(t) = \boldsymbol{B}^*\boldsymbol{\tau},
\end{aligned}
\tag{33}
$$

where

- matrices with k in the subscript refer to the structurally known part of the dynamics model,

- matrices with 0 in the subscript refer to the fully known part of the robot dynamics,

- matrices with ρ in the subscript refer to the parametrically unknown part of the model dynamics and they are rewritten as matrix $\boldsymbol{Y}$,

- $\boldsymbol{Y} \in \mathbb{R}^{(m+p)\times r}$ is the regression matrix describing the linear dependence on the unknown parameters,

- $\rho \in \mathbb{R}^r$ is the vector of unknown dynamic parameters, and

- $\zeta \in \mathbb{R}^{m+p}$ represents all unknown impacts which influence the robot and are treated as slow-varying disturbances. They cover both uncertainties in the internal structure of the robot dynamics and neglected external factors, such as limited acting forces or an environment impact on friction forces, e.g., temperature, air viscosity.

In order to define a sliding control law, it is assumed that the unknown parameters and disturbances are bounded and the limits are known:

- $|\rho_i| \leq \rho_i^*$, $i = 1, 2, \dots, r$,

- $|\zeta_i(t)| \leq \zeta_i^*$, $i = 1, 2, \dots, m + p$.

The upper limits of the parametric and structural uncertainties can be estimated, at least roughly, based on the available data in a robot manual (permissible load, maximum velocities) and knowledge of the work environment (predictable order of magnitude of mass elements, friction, or external forces).

The following dynamic control law is proposed:

$$
\begin{aligned}
\boldsymbol{\tau} = (\boldsymbol{B}^*)^{-1} \Big(&\boldsymbol{Q}_0^*(\boldsymbol{q})\dot{\boldsymbol{z}}_{\mathrm{dyn}} + \boldsymbol{C}_0^*(\boldsymbol{q}, \dot{\boldsymbol{q}})\boldsymbol{z}_{\mathrm{dyn}} \\
&+ \boldsymbol{D}_0^*(\boldsymbol{q}) + \boldsymbol{Y}_d(\dot{\boldsymbol{z}}_{\mathrm{dyn}}, \boldsymbol{z}_{\mathrm{dyn}}, \dot{\boldsymbol{q}}, \boldsymbol{q})\hat{\boldsymbol{\rho}} - \boldsymbol{C}_0^\gamma(\dot{\boldsymbol{q}}, \boldsymbol{q})\boldsymbol{\sigma} \\
&- \boldsymbol{X}_\sigma(\boldsymbol{\sigma}, \dot{\boldsymbol{q}}, \boldsymbol{q})\hat{\boldsymbol{\rho}} - \boldsymbol{K}_d\boldsymbol{\sigma} - \boldsymbol{K}\mathrm{sgn}(\boldsymbol{\sigma}) \Big),
\end{aligned}
\tag{34}
$$

where

- σ is the slide variable defined as

$$
\boldsymbol{\sigma} = \boldsymbol{e_z} + \boldsymbol{\Lambda}\boldsymbol{e} = \boldsymbol{z} - \boldsymbol{z}_{\mathrm{dyn}}
\tag{35}
$$

  with $\boldsymbol{\Lambda}$ as a positive-definite diagonal matrix and the error signal $\boldsymbol{e}(t)$ satisfying the following relations

$$
\boldsymbol{e}(t) = \int_0^t \boldsymbol{e_z}(u)\, \mathrm{d}u,
\tag{36a}
$$
$$
\dot{\boldsymbol{e}}(t) = \boldsymbol{e_z}(t);
\tag{36b}
$$

- $\boldsymbol{z}_{\mathrm{dyn}}$ is the reference signal defined based on the velocity profiles generated on the kinematics level and results from the slide variable definition

$$
\boldsymbol{z}_{\mathrm{dyn}} = \boldsymbol{z}_{\mathrm{ref}} - \boldsymbol{\Lambda}\boldsymbol{e};
\tag{37}
$$

- d in the subscript of the regression matrix $\boldsymbol{Y}_d$ means that it depends on the reference signals $\dot{\boldsymbol{z}}_{\mathrm{dyn}}$ and $\boldsymbol{z}_{\mathrm{dyn}}$;

- $\boldsymbol{X}_\sigma \in \mathbb{R}^{(m+p)\times r}$ is the regression matrix describing the linear dependence of the correction matrix, defined by Eqn. (8), on the unknown parameters $\boldsymbol{\rho}$. It satisfies the relation

$$
\boldsymbol{X}_\sigma(\boldsymbol{\sigma}, \dot{\boldsymbol{q}}, \boldsymbol{q})\boldsymbol{\rho} = \boldsymbol{C}_{\boldsymbol{\rho}}^\gamma(\dot{\boldsymbol{q}}, \boldsymbol{q}, \boldsymbol{\rho})\boldsymbol{\sigma};
$$

- $\boldsymbol{C}_0^\gamma \in \mathbb{R}^{(m+p)\times(m+p)}$ is the part of the correction matrix which is known structurally and parametrically. Together with the part dependant on the unknown parameters, $\boldsymbol{C}_{\boldsymbol{\rho}}^\gamma$, it creates the correction matrix

$$
\boldsymbol{C}_k^\gamma(\dot{\boldsymbol{q}}, \boldsymbol{q}, \boldsymbol{\rho}) = \boldsymbol{C}_0^\gamma(\dot{\boldsymbol{q}}, \boldsymbol{q}) + \boldsymbol{C}_{\boldsymbol{\rho}}^\gamma(\dot{\boldsymbol{q}}, \boldsymbol{q}, \boldsymbol{\rho})
$$

  to satisfy Property 1 for the structurally known matrices, i.e., $\boldsymbol{Q}_k^*(\boldsymbol{q}, \boldsymbol{\rho})$ and $\boldsymbol{C}_k^*(\dot{\boldsymbol{q}}, \boldsymbol{q}, \boldsymbol{\rho})$;

- $\hat{\boldsymbol{\rho}}$ is the estimation of the unknown parameters. It is constant and selected from the known range before the control process;

- $\boldsymbol{K}_d$ is the symmetric and positive-definite gain matrix;

- $K = \mathrm{diag}\{k_i\}$, $i = 1, 2, \ldots, m + p$ is a diagonal matrix.

Let us notice that the expression $K\mathrm{sgn}(\boldsymbol{\sigma})$ is responsible for compensating errors resulting from the lack of knowledge of the model. It attracts the system to the sliding surface where the system dynamics converges to the origin. The proposed approach results in correct path following as stated by the following result:

Theorem 2. *The system* (33) *in the closed feedback loop with the control law* (34) *is asymptotically stable at the zero equilibrium point. Hence, the error signals, e_z and e_ξ, converge to zero asymptotically.*

Proof. (Dynamic control law) The system (33) in the closed feedback loop with the control law (34) is expressed with the equation

$$\begin{aligned}
\boldsymbol{Q}_0^*\dot{\boldsymbol{z}} + \boldsymbol{C}_0^*\boldsymbol{z} + \boldsymbol{D}_0^* + \boldsymbol{Y}\boldsymbol{\rho} + \boldsymbol{\zeta} \\
= \boldsymbol{Q}_0^*\dot{\boldsymbol{z}}_{\mathrm{dyn}} + \boldsymbol{C}_0^*\boldsymbol{z}_{\mathrm{dyn}} + \boldsymbol{D}_0^* + \boldsymbol{Y}_d\hat{\boldsymbol{\rho}} \\
- \boldsymbol{C}_0^\gamma\boldsymbol{\sigma} - \boldsymbol{X}_\sigma\hat{\boldsymbol{\rho}} - \boldsymbol{K}_d\boldsymbol{\sigma} - \boldsymbol{K}\mathrm{sgn}(\boldsymbol{\sigma}),
\end{aligned} \quad (38)$$

where the matrix arguments are omitted for the clarity of notation. Let us subtract the elements $\boldsymbol{Y}_d\boldsymbol{\rho}$ and $\boldsymbol{X}_\sigma\boldsymbol{\rho}$ from both the sides of Eqn. (38). We obtain

$$\begin{aligned}
\boldsymbol{Q}_k^*\dot{\boldsymbol{\sigma}} + \boldsymbol{C}_k^*\boldsymbol{\sigma} - \boldsymbol{Z}\tilde{\boldsymbol{\rho}} + \boldsymbol{C}_k^\gamma\boldsymbol{\sigma} \\
+ \boldsymbol{K}_d\boldsymbol{\sigma} + \boldsymbol{K}\mathrm{sgn}(\boldsymbol{\sigma}) + \boldsymbol{\zeta} = 0,
\end{aligned} \quad (39)$$

where $\tilde{\boldsymbol{\rho}} = \hat{\boldsymbol{\rho}} - \boldsymbol{\rho}$ is the error of unknown parameters estimation and $\boldsymbol{Z} = \boldsymbol{Y}_d - \boldsymbol{X}_\sigma$.

Notice that the considered disturbances consist of disturbances resulting from the lack of the knowledge of the inertia matrix structure, Coriolis and centrifugal forces matrix structures, and other disturbances, i.e., $\boldsymbol{\zeta} = \boldsymbol{\zeta}_Q + \boldsymbol{\zeta}_C + \boldsymbol{\zeta}_R$. According to the assumptions, all of the elements are bounded. Hence, the fully known matrices along the system trajectories are obtained

$$\boldsymbol{Q}^*\dot{\boldsymbol{z}} = \boldsymbol{Q}_k^*\dot{\boldsymbol{z}} + \boldsymbol{\zeta}_Q, \quad \boldsymbol{C}^*\boldsymbol{z} = \boldsymbol{C}_k^*\boldsymbol{z} + \boldsymbol{\zeta}_C. \quad (40)$$

In a similar way, matrices along the reference trajectories can be denoted as

$$\begin{aligned}
\boldsymbol{Q}^*\dot{\boldsymbol{z}}_{\mathrm{dyn}} = \boldsymbol{Q}_k^*\dot{\boldsymbol{z}}_{\mathrm{dyn}} + \boldsymbol{\zeta}_{Q_d}, \\
\boldsymbol{C}^*\boldsymbol{z}_{\mathrm{dyn}} = \boldsymbol{C}_k^*\boldsymbol{z}_{\mathrm{dyn}} + \boldsymbol{\zeta}_{C_d}.
\end{aligned} \quad (41)$$

Moreover, we denote by $\boldsymbol{\zeta}_\gamma$ and $\boldsymbol{\zeta}_{\gamma_d}$ the structurally unknown parts of the correction matrix along the system and along the reference trajectories, respectively. They may exist due to structurally unknown elements of the robot dynamics as the matrix $\boldsymbol{C}_k^*$ was defined only on the structurally known part. Thus,

$$\begin{aligned}
\boldsymbol{C}^\gamma\boldsymbol{z} = \boldsymbol{C}_k^\gamma\boldsymbol{z} + \boldsymbol{\zeta}_\gamma, \\
\boldsymbol{C}^\gamma\boldsymbol{z}_{\mathrm{dyn}} = \boldsymbol{C}_k^\gamma\boldsymbol{z}_{\mathrm{dyn}} + \boldsymbol{\zeta}_{\gamma_d}.
\end{aligned} \quad (42)$$

The matrix $\boldsymbol{C}^\gamma$ satisfies Property 1 for the complete matrices, i.e., $\boldsymbol{Q}^*$ and $\boldsymbol{C}^*$. Taking into account the above relations, Eqn. (39) is reformulated as

$$\begin{aligned}
\boldsymbol{Q}^*\dot{\boldsymbol{\sigma}} + \boldsymbol{C}^*\boldsymbol{\sigma} - \boldsymbol{Z}\tilde{\boldsymbol{\rho}} + \boldsymbol{C}^\gamma\boldsymbol{\sigma} \\
+ \boldsymbol{K}_d\boldsymbol{\sigma} + \boldsymbol{K}\mathrm{sgn}(\boldsymbol{\sigma}) + \boldsymbol{\zeta}_N = 0,
\end{aligned} \quad (43)$$

where $\boldsymbol{\zeta}_N = \boldsymbol{\zeta}_R + \boldsymbol{\zeta}_{Q_d} + \boldsymbol{\zeta}_{C_d} - \boldsymbol{\zeta}_\gamma + \boldsymbol{\zeta}_{\gamma_d}$.

Consider a Lypunov-like candidate function

$$V_2(\boldsymbol{e}_\xi, \boldsymbol{\sigma}, \boldsymbol{e}_z, t) = V_1(\boldsymbol{e}_\xi) + \frac{1}{2}\boldsymbol{\sigma}^T\boldsymbol{Q}^*\boldsymbol{\sigma}, \quad (44)$$

which is always non-negative due to the properties of the inertia matrix $\boldsymbol{Q}^*$ and the function V_1 defined by Eqn. (29).

The time derivative of the function (44) along the system trajectories is equal to

$$\dot{V}_2 = \dot{V}_1 + \boldsymbol{\sigma}^T\boldsymbol{Q}^*\dot{\boldsymbol{\sigma}} + \frac{1}{2}\boldsymbol{\sigma}^T\dot{\boldsymbol{Q}}^*\boldsymbol{\sigma}. \quad (45)$$

Taking into account Eqns. (8) and (43), we get

$$\begin{aligned}
\dot{V}_2 = \dot{V}_1 - \boldsymbol{\sigma}^T\boldsymbol{K}_d\boldsymbol{\sigma} \\
- \boldsymbol{\sigma}^T(\boldsymbol{K}\mathrm{sgn}(\boldsymbol{\sigma}) + \boldsymbol{\zeta}_N - \boldsymbol{Z}\tilde{\boldsymbol{\rho}}).
\end{aligned} \quad (46)$$

It can be observed that the last component of the sum in Eqn. (46) is equal to

$$\begin{aligned}
\boldsymbol{\sigma}^T(\boldsymbol{K}\mathrm{sgn}(\boldsymbol{\sigma}) + \boldsymbol{\zeta}_N - \boldsymbol{Z}\tilde{\boldsymbol{\rho}}) \\
= \sum_{i=1}^{m+p} |\sigma_i|\Big(k_i + \zeta_{N_i}\mathrm{sgn}(\sigma_i) - \sum_{j=1}^{r} Z_{ij}\tilde{\rho}_j\mathrm{sgn}(\sigma_i)\Big).
\end{aligned} \quad (47)$$

Define

$$k_i = \sum_{j=1}^{r} Z_{ij}^*\alpha_j + \zeta_{N_i}^* + \delta_i, \quad (48)$$

where $|Z_{ij}| \leq Z_{ij}^*$ expresses the model constraints along the system trajectories and reference trajectories, $\alpha_j = |\hat{\rho}_j| + \rho_j^* \geq |\tilde{\rho}_j|$ constitutes the evaluation of the maximal estimation error of the unknown parameters, δ_i is a positive number, and $\zeta_{N_i}^*$ is the upper limit of the unknown disturbances, i.e.,

$$\begin{aligned}
|\zeta_{N_i}| \leq |\zeta_{R_i}| + |\zeta_{Q_{d_i}}| + |\zeta_{C_{d_i}}| \\
+ |\zeta_{\gamma_{d_i}} - \zeta_{\gamma_i}| \leq \zeta_{N_i}^*,
\end{aligned}$$

$i = 1, 2, \ldots, m + p$. The newly defined disturbances $\boldsymbol{\zeta}_N$ are bounded as they comprise the disturbances limited by assumption and constrained reference trajectories. We can notice that for $i = 1, 2, \ldots, m + p$

$$\sum_{j=1}^{r} Z_{ij}^*\alpha_j - \sum_{j=1}^{r} Z_{ij}\tilde{\rho}_j\mathrm{sgn}(\sigma_i) \geq 0, \quad (49a)$$

$$\zeta_{N_i}^* + \zeta_{N_i}\mathrm{sgn}(\sigma_i) \geq 0. \quad (49b)$$

From the definition (48) and the relations (49) it may be concluded that

$$\dot{V}_2 \leq \dot{V}_1(\boldsymbol{e}_{\boldsymbol{\xi}}) - \boldsymbol{\sigma}^T \boldsymbol{K}_d \boldsymbol{\sigma} - \sum_{i=1}^{m+p} \delta_i |\sigma_i|$$
$$= \dot{V}_1(\boldsymbol{e}_{\boldsymbol{\xi}}) - W_2(\boldsymbol{\sigma}) \leq 0. \quad (50)$$

Notice that the element $W_2(\boldsymbol{\sigma}) = \boldsymbol{\sigma}^T \boldsymbol{K}_d \boldsymbol{\sigma} + \sum_{i=1}^{m+p} \delta_i |\sigma_i|$ is non-negative for any positive-definite matrix $\boldsymbol{K}_d$. It is clear that

$$W_2(\boldsymbol{\sigma}) = 0 \iff \boldsymbol{\sigma} = \boldsymbol{0}. \quad (51)$$

Hence, the LaSalle–Yoshizawa theorem (Canudas de Wit *et al.*, 1996) is harnessed to conclude that the trajectories of the system (38) tend to zero asymptotically for the positive-definite matrix $\boldsymbol{K}_d$ and the matrix $\boldsymbol{K}$ defined by Eqn. (48). The trajectories of the system are brought to the sliding surface. As a result, based on Eqns. (35), (36b), and (51), the following relation is obtained:

$$\boldsymbol{e_z} = \dot{\boldsymbol{e}} = -\boldsymbol{\Lambda} \boldsymbol{e}, \quad (52)$$

which for the positive-definite matrix $\boldsymbol{\Lambda}$ means that $\boldsymbol{e} \to \boldsymbol{0}$ as $t \to +\infty$. As a consequence, also $\boldsymbol{z} \to \boldsymbol{z}_{\text{ref}}$ as $t \to +\infty$, so that the velocity profiles generated on the kinematics level are followed asymptotically. Due to the facts that the first level of the control cascade was taken into account in the definition of the function (44) and the errors $\boldsymbol{e}_{\boldsymbol{\xi}}$ and $\boldsymbol{e_z}$ are coupled, we deduce that both error signals converge to zero and the path is followed correctly.

∎

7. Simulation results

In this section results of the simulation study for a particular model of the mobile manipulator are presented.

7.1. Controlled robot. The plant considered in the simulation study is a mobile manipulator of the type (nh, h), which is presented in Fig. 4. It consists of a unicycle-like platform of the type $(2, 0)$ (Campion *et al.*, 1996) and an RTR manipulator mounted on the platform. The robotic arm has three degrees of freedom: rotational, translational and rotational. Parameters of the mobile manipulator taken into account during the simulation study are presented in Table 1. Mobile platform parameters are based on the vehicle considered by Yamamoto and Yun (1996), while the manipulator description is chosen arbitrarily.

The state of the platform is $\boldsymbol{q}_m = \begin{pmatrix} x & y & \phi \end{pmatrix}^T$, which describes its position $\begin{pmatrix} x & y \end{pmatrix}^T$ and orientation ϕ on the $X_0 Y_0$ plane. In turn, $\boldsymbol{q}_r = \begin{pmatrix} q_1 & q_2 & q_3 \end{pmatrix}^T$
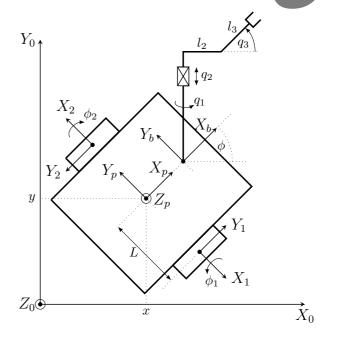

Fig. 4. Schematic view of the mobile manipulator.

is the robotic arm state, which describes positions in the respective joints. The initial state of the mobile manipulator was arbitrarily chosen as

$$\boldsymbol{q}_0 = \begin{pmatrix} 0.5\text{m} & 0 & 0 & \frac{\pi}{4}\text{rad} & 0.5\text{m} & -\frac{\pi}{2}\text{rad} \end{pmatrix}^T,$$
$$(53)$$

while the initial auxiliary velocities are equal to $\boldsymbol{z}_0 = \boldsymbol{0}$.

7.2. Control law description. In this section the elements of the control law considered in the simulation study are described. The selection is exemplary to verify the performance of the proposed algorithm.

The desired path was defined as a straight line, which is the most evident example of a zero-curvature path. It was given with the equation

$$\boldsymbol{r}(s) = \boldsymbol{r}_0 + s \frac{\boldsymbol{T}_0}{\|\boldsymbol{T}_0\|}, \quad (54)$$

where $\boldsymbol{r}_0 = \begin{pmatrix} 1 & 0.1 & 0.15 \end{pmatrix}^T$, $\boldsymbol{T}_0 = \begin{pmatrix} 1 & 1 & 0.05 \end{pmatrix}^T$. The desired value of vector $\boldsymbol{\xi}_d$ was defined as

$$\boldsymbol{\xi}_d(t) = \begin{pmatrix} 0.1t + s_0 & 0 & 0 \end{pmatrix}^T, \quad (55)$$

where s_0 is the initial value of the curvilinear distance resulting from the orthogonal projection of the object onto the curve.

In the conducted numerical analysis the following control gains were chosen arbitrarily:

- kinematic controller: $\boldsymbol{K}_k = \text{diag}_{3\times 3}\{100\}$;

- dynamic controller: $\boldsymbol{K}_d = \text{diag}_{5\times 5}\{200\}$, $\boldsymbol{K} = \text{diag}_{5\times 5}\{10\}$, $\boldsymbol{\Lambda} = \text{diag}_{5\times 5}\{0.1\}$.

Table 1. Mobile manipulator parameters.

Symbol	Value	Description
M_p	94 kg	mobile platform mass
M_k	5 kg	wheel mass
R	0.075 m	wheel radius
I_Z	$6.609\,\text{kg}\cdot\text{m}^2$	inertia moment of the platform with respect to the Z_p axis of its local frame
L	0.3 m	half width of the mobile platform
l	0.2 m	distance between manipulator base and platform centre of mass in the X_p axis of the platform local frame
l_2	0.3 m	length of 2$^\text{nd}$ manipulator link
l_3	0.2 m	length of 3$^\text{rd}$ manipulator link
m_2	20 kg	mass of manipulator link l_2
m_3	20 kg	mass of manipulator link l_3

Fig. 5. Path followed by the mobile manipulator.
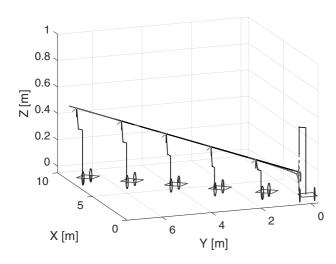

Fig. 6. Path following errors.

Moreover, in the simulation study some parametric and structural uncertainties were artificially introduced to validate the performance of the sliding mode controller (34). In the case of parametric uncertainty, four parameters were assumed to be unknown

$$\boldsymbol{\rho} = \begin{pmatrix} m_3 l_2 l_3 & m_3 l_2^2 & I_p/L^2 & m_3 l_2 \end{pmatrix}^T,$$

where $I_p = I_Z + 0.5 M_k R^2 + 2 M_k L^2$ is the total inertia moment of the mobile robot with respect to Z_p axis of its local frame, see Fig. 4. In the control law the following constant values of parameters were assumed: $\hat{\boldsymbol{\rho}} = \begin{pmatrix} 1 & 5 & 60 & 10 \end{pmatrix}^T$. It is noteworthy that the chosen values of unknown parameters $\hat{\boldsymbol{\rho}}$ were different from the real values. Finally, some parts of the dynamic model structure were neglected to verify the impact of structural uncertainties. It simulates the lack of knowledge or errors made in the modelling process. The arbitrarily selected elements were equal to zero in the control law, although they are non-zero values in the robot dynamics (7). The omitted elements were chosen as follows:
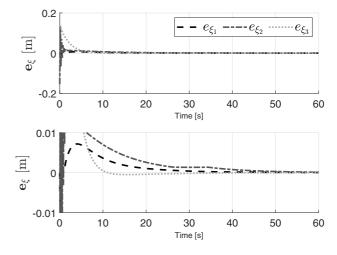
- The whole gravity terms vector $\boldsymbol{D}^*$; hence, $\boldsymbol{D}_k^* = \boldsymbol{0}$ in Eqn. (33).

- Two elements on the main diagonal of the inertia matrix. They correspond to the translational and second rotational joints of the robotic arm, namely Q_{44}^* and Q_{55}^*. They are part of the matrix $\boldsymbol{Q}_{22}$ in Eqn. (7). As a result, the matrix $\boldsymbol{Q}_k^*$ in Eqn. (33) is equal to

$$\boldsymbol{Q}_k^* = \begin{bmatrix} \boldsymbol{G}^T \boldsymbol{Q}_{11} \boldsymbol{G} & \boldsymbol{G}^T \boldsymbol{Q}_{12} \\ \boldsymbol{Q}_{21} \boldsymbol{G} & \begin{bmatrix} Q_{33}^* & Q_{34}^* & Q_{35}^* \\ Q_{34}^* & 0 & Q_{45}^* \\ Q_{35}^* & Q_{45}^* & 0 \end{bmatrix} \end{bmatrix}.$$

The remaining elements of the controllers were derived according to the dynamic and kinematic models of the considered mobile manipulator.
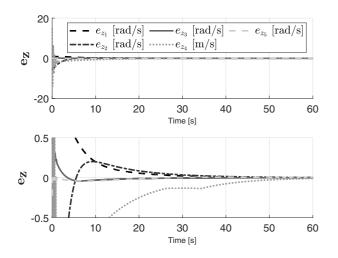
Fig. 7. Velocity profile following errors.

Fig. 8. Control signals.

7.3. Numerical results. In order to verify the theoretical results presented in the previous sections, numerical simulations for the defined robot were conducted in the MATLAB environment. The direct-drive system was considered. Also, it was assumed that all necessary measurements are available directly. In Fig. 5 the desired path and the path performed by the mobile manipulator are shown. The control system compensates the initial error, and forces the robot to approach the path and move along the curve.

This behaviour can be even better observed in graphs presenting the path following errors (Fig. 6) and the velocity profile following errors (Fig. 7). All errors asymptotically converge to zero. This confirms the properties of the algorithm proven with the theoretical analysis. In the transient state some high-frequency oscillations can be observed. They result from the signum element considered in the control law. However, when the robot is close to the path, the error signals converge to zero smoothly.

Finally, in Fig. 8 control signals generated by the dynamic controller are presented. It is worth noticing that the sliding mode controller introduces some rapid changes in the control signals in order to compensate the lack of knowledge of the dynamic model. It leads to oscillations of the control value (in particular τ_3) or sudden changes of the value level (τ_4 approximately in the middle of the simulation time). It is worth noticing that the impact of the sliding mode controller can be especially observed in the degrees of freedom where elements of the dynamic model structure were neglected. Furthermore, the highest values are generated in the transient state. They are responsible for compensating the error resulting from the initial state and change quite fast. It is the result of the non-continuous element of the control law and choice of the control gains.
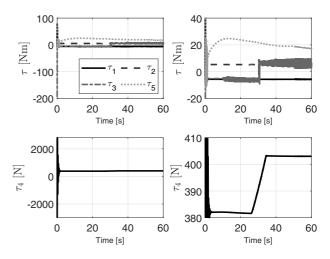
8. Conclusions

In the paper the robust path following algorithm has been presented. It offers the following features:

1. It is based on the Bishop parametrization. This means that the algorithm is robust to all zero-curvature points as the local frame on the path is always well defined.

2. The robot is projected onto the path using the orthogonal projection method which minimizes the problem dimensionality. We proposed the orthogonal projection constraint in such a form that the resulting singularity is outside the path. Therefore, the presented algorithm allows the robot to reach the path and moves along it. It is noteworthy that the presented solution is not restricted only to the one type of a path. Any curve satisfying the Bishop parametrization assumptions can be commanded as the desired path.

3. The control law has been designed based on the backstepping method. The sliding mode controller, considered at the dynamics level, guarantees robustness to the parametric and structural uncertainties of the dynamics model.

4. The proposed control law is characterised with the asymptotic convergence of errors to zero, which is proven analytically.

The conducted simulation study confirms the theoretical results and properties of the presented algorithm. However, it has to be noticed that too high control gains for the sliding mode controller may lead to high amplitudes and high-frequency changes of the control signals. Thus, the dynamic model structure has

to be identified as precisely as possible in order to avoid signals which may destroy a physical object. The more knowledge we have about the dynamics model, the lower gains can be used in the sliding mode controller. Although the control algorithm is robust to uncertainties of the dynamic model, it may require unfeasible actuations to compensate them in case of enormous differences between the real robot and the model considered in the control law.

All in all, in the paper we proposed the parametric-based path following algorithm which is a generalization of the path following methods for mobile manipulators. The achieved results indicate further research directions. The control of the end-effector orientation with respect to a moving reference frame should be additionally considered. Moreover, the control constraints may be explicitly taken into account in the control law. Finally, the control law should be validated experimentally on a real mobile manipulator. The authors have already validated path following algorithms for a fixed-base manipulator, e.g., (Dyba, 2023; 2024). The laboratory test-bed equipped with the mobile manipulator is under construction and will be used in the future investigation.

References

Abadi, A.S.S., Hosseinabadi, P.A., Mekhilef, S. and Ordys, A. (2020). A new strongly predefined time sliding mode controller for a class of cascade high-order nonlinear systems, *Archives of Control Sciences* **30**(3): 599–620, DOI: 10.24425/acs.2020.134679.

Bartoszewicz, A. and Adamiak, K. (2019). A reference trajectory based discrete time sliding mode control strategy, *International Journal of Applied Mathematics and Computer Science* **29**(3): 517–525, DOI: 10.2478/amcs-2019-0038.

Bishop, R.L. (1975). There is more than one way to frame a curve, *The American Mathematical Monthly* **82**(3): 246–251, DOI: 10.2307/2319846.

Campion, G., Bastin, G. and D'Andréa-Novel, B. (1996). Structural properties and classification of kinematic and dynamic models of wheeled mobile robots, *IEEE Transactions on Robotics and Automation* **12**: 47–61, DOI: 10.1109/70.481750.

Canudas de Wit, C., Bastin, G. and Siciliano, B. (1996). *Theory of Robot Control*, 1st edn, Springer, London.

Carroll, D., Köse, E. and Sterling, I. (2013). Improving Frenet's frame using Bishop's frame, *Journal of Mathematics Research* **5**: 97–106, DOI:10.5539/jmr.v5n4p97.

Cichella, V., Kaminer, I., Xargay, E., Dobrokhodov, V., Hovakimyan, N., Aguiar, A.P. and Pascoal, A.M. (2012). A Lyapunov-based approach for time-coordinated 3D path-following of multiple quadrotors, *Proceedings of the 51st Annual IEEE Conference on Decision and Control, Maui, Hawaii, USA*, pp. 1776–1781.

Costa, M.M. and Silva, M.F. (2019). A survey on path planning algorithms for mobile robots, *2019 IEEE International Conference on Autonomous Robot Systems and Competitions (ICARSC), Porto, Portugal*, pp. 1–7, DOI: 10.1109/ICARSC.2019.8733623.

Dulęba, I. (2000). Modeling and control of mobile manipulators, *IFAC Proceedings Volumes* **33**(27): 447–452, DOI: 10.1016/S1474-6670(17)37970-3.

Dyba, F. (2023). Experimental validation of the non-orthogonal Serret-Frenet parametrization applied to the path following task, *Proceedings of the 20th International Conference on Informatics in Control, Automation and Robotics - Volume 1: ICINCO, Rome, Italy*, pp. 608–615, DOI: 10.5220/0012164200003543.

Dyba, F. (2024). Parallel position and orientation control for a redundant manipulator performing the path following task, *13th International Workshop on Robot Motion and Control (RoMoCo), Poznan, Poland*, pp. 199–204, DOI: 10.1109/RoMoCo60539.2024.10604337.

Dyba, F. and Mazur, A. (2024). Comparison of curvilinear parametrization methods and avoidance of orthogonal singularities in the path following task, *Journal of Automation, Mobile Robotics and Intelligent Systems* **17**(3): 46–64, DOI: 10.14313/JAMRIS/3-2023/22.

Encarnação, P. and Pascoal, A. (2000). 3D path following for autonomous underwater vehicle, *Proceedings of the 39th IEEE Conference on Decision and Control*, Vol. 3, Sydney, NSW, Australia, pp. 2977–2982, DOI: 10.1109/CDC.2000.914272.

Frenet, F. (1852). Sur les courbes à double courbure, *Journal de Mathématiques Pures et Appliquées,* **17**: 437–447, http://eudml.org/doc/233946.

Galicki, M. (2006). Adaptive control of kinematically redundant manipulator along a prescribed geometric path, in K. Kozłowski (Ed.), *Robot Motion and Control*, Lecture Notes in Control and Information Sciences, Vol. 335, Springer, London, pp. 129–139.

Gonçalves, V.M., Adorno, B.V., Crosnier, A. and Fraisse, P. (2020). Stable-by-design kinematic control based on optimization, *IEEE Transactions on Robotics* **36**(3): 644–656, DOI: 10.1109/TRO.2019.2963665.

Gonçalves, V.M., Pimenta, L.C.A., Maia, C.A., Dutra, B.C.O. and Pereira, G.A.S. (2010). Vector fields for robot navigation along time-varying curves in n-dimensions, *IEEE Transactions on Robotics* **26**(4): 647–659, DOI: 10.1109/TRO.2010.2053077.

Hung, N., Rego, F., Quintas, J., Cruz, J., Jacinto, M., Souto, D., Potes, A., Sebastiao, L. and Pascoal, A. (2023). A review of path following control strategies for autonomous robotic vehicles: Theory, simulations, and experiments, *Journal of Field Robotics* **40**(3): 747–779, DOI: 10.1002/rob.22142.

Jafarzadeh, H. and Fleming, C. H. (2018). An exact geometry–based algorithm for path planning, *International Journal of Applied Mathematics and Computer Science* **28**(3): 493–504, DOI: 10.2478/amcs-2018-0038.

Kapitanyuk, Y.A., Proskurnikov, A.V. and Cao, M. (2018). A guiding vector-field algorithm for path-following control of nonholonomic mobile robots, *IEEE Transactions on Control Systems Technology* **26**(4): 1372–1385, DOI: 10.1109/TCST.2017.2705059.

Kozłowski, K. and Pazderski, D. (2004). Modeling and control of a 4-wheel skid-steering mobile robot, *International Journal of Applied Mathematics and Computer Science* **14**(4): 477–496.

Krstić, M., Kanellakopoulos, I. and Kokotović, P.V. (1995). *Nonlinear and Adaptive Control Design*, Wiley, New York, USA.

Lee, J.M. (1997). *Riemannian Manifolds: An Introduction to Curvature*, Springer, New York.

Li, X., Zhao, G. and Li, B. (2020). Generating optimal path by level set approach for a mobile robot moving in static/dynamic environments, *Applied Mathematical Modelling* **85**: 210–230, DOI: 10.1016/j.apm.2020.03.034.

Liao, Y.-L., Zhang, M.-J. and Wan, L. (2015). Serret–Frenet frame based on path following control for underactuated unmanned surface vehicles with dynamic uncertainties, *Journal of Central South University* **22**: 214–223, DOI: 10.1007/s11771-015-2512-z.

Liu, H. and Pei, D. (2013). Singularities of a space curve according to the relatively parallel adapted frame and its visualization, *Mathematical Problems in Engineering* **2013**(512020): 1–12, DOI: 10.1155/2013/512020.

Lugo-Cárdenas, I., Salazar, S. and Lozano, R. (2017). Lyapunov based 3D path following kinematic controller for a fixed wing UAV, *IFAC-PapersOnLine* **50**(1): 15946–15951, DOI: 10.1016/j.ifacol.2017.08.1747.

Mazur, A. (2004). Hybrid adaptive control laws solving a path following problem for non-holonomic mobile manipulators, *International Journal of Control* **77**(15): 1297–1306, DOI: 10.1080/0020717042000297162.

Mazur, A. (2010). Trajectory tracking control in workspace-defined tasks for nonholonomic mobile manipulators, *Robotica* **28**(1): 57–68, DOI: 10.1017/S0263574709005578.

Mazur, A. and Dyba, F. (2023). The non-orthogonal serret–frenet parametrization applied to the path following problem of a manipulator with partially known dynamics, *Archives of Control Sciences* **33**(2): 339–370, DOI: 10.24425/acs.2023.146279.

Mazur, A. and Płaskonka, J. (2012). The Serret–Frenet parametrization in a control of a mobile manipulator of (nh, h) type, *IFAC Proceedings Volumes* **45**(22): 405–410, DOI: 10.3182/20120905-3-HR-2030.00069.

Mazur, A., Płaskonka, J. and Kaczmarek, M. (2015). Following 3D paths by a manipulator, *Archives of Control Sciences* **25**(1): 117–133, DOI: 10.1515/acsc-2015-0008.

Mazur, A. and Szakiel, D. (2009). On path following control of nonholonomic mobile manipulators, *International Journal of Applied Mathematics and Computer Science* **19**(4): 561–574.

Micaelli, A. and Samson, C. (1993). Trajectory tracking for unicycle-type and two-steering-wheels mobile robots, *Technical Report No. 2097*, INRIA, Sophia-Antipolis.

Michałek, M. and Kozłowski, K. (2009). Motion planning and feedback control for a unicycle in a way point following task: The VFO approach, *International Journal of Applied Mathematics and Computer Science* **19**(4): 533–545, DOI: 10.1007/s10846-017-0482-0.

Michałek, M.M. and Gawron, T. (2018). VFO Path following control with guarantees of positionally constrained transients for unicycle-like robots with constrained control input, *Journal of Intelligent and Robotic Systems: Theory and Applications* **89**(1-2): 191 – 210.

Oprea, J. (1997). *Differential Geometry and Its Applications*, Prentice Hall, Michigan University.

Pepy, R., Kieffer, M. and Walter, E. (2009). Reliable robust path planning with application to mobile robots, *International Journal of Applied Mathematics and Computer Science* **19**(3): 413–424, DOI: 10.2478/v10006-009-0034-2.

Przybylski, M. and Putz, B. (2017). D* Extra Lite: A dynamic A* with search–tree cutting and frontier–gap repairing, *International Journal of Applied Mathematics and Computer Science* **27**(2): 273–290, DOI: 10.1515/amcs-2017-0020.

Rezende, A.M.C., Goncalves, V.M. and Pimenta, L.C.A. (2022). Constructive time-varying vector fields for robot navigation, *IEEE Transactions on Robotics* **38**(2): 852–867, DOI: 10.1109/TRO.2021.3093674.

Selig, J.M. and Wu, Y. (2006). Interpolated rigid-body motions and robotics, *2006 IEEE/RSJ International Conference on Intelligent Robots and Systems, Beijing, China*, pp. 1086–1091, DOI: 10.1109/IROS.2006.281815.

Serret, J.-A. (1851). Sur quelques formules relatives à la théorie des courbes à double courbure, *Journal de Mathématiques Pures et Appliquées,* **16**: 193–207.

Slotine, J.-J. and Li, W. (1991). *Applied Nonlinear Control*, Prentice Hall, Englewood Cliffs, N.J.

Soetanto, D., Lapierre, L. and Pascoal, A. (2003). Adaptive, non-singular path-following control of dynamic wheeled robots, *Proceedings of the 42nd IEEE International Conference on Decision and Control*, Vol. 2, Maui, HI, pp. 1765–1770, DOI: 10.1109/CDC.2003.1272868.

Spong, M. and Vidyasagar, M. (1991). *Robot Dynamics and Control*, Wiley, New York.

Sun, K. and Liu, X. (2021). Path planning for an autonomous underwater vehicle in a cluttered underwater environment based on the heat method, *International Journal of Applied Mathematics and Computer Science* **31**(2): 289–301, DOI: 10.34768/amcs-2021-0019.

Utkin, V.I. (1992). *Sliding Modes in Control and Optimization*, Springer, Berlin.

Yamamoto, Y. and Yun, X. (1996). Effect of the dynamic interaction on coordinated control of mobile manipulators, *IEEE Transactions on Robotics and Automation* **12**(5): 816–824, DOI: 10.1109/70.538986.

Yao, W., de Marina, H.G., Lin, B. and Cao, M. (2021). Singularity-free guiding vector field for robot navigation, *IEEE Transactions on Robotics* **37**(4): 1206–1221, DOI: 10.1109/TRO.2020.3043690.

Alicja Mazur received her MS and PhD degrees in control engineering and robotics from the Wroclaw University of Science and Technology (Wrocław Tech), Poland, in 1990 and 1997, respectively. In 2011 she received her DSc degree from the Łódź University of Technology. She is currently a professor at the Faculty of Electronics, Fotonics and Microsystems at Wrocław Tech, Poland. Her research interests include robotics, aerospace engineering, non-linear, adaptive and robust control systems, pattern recognition and differential geometry.

Filip Dyba received his MS degree in control engineering and robotics from the Wroclaw University of Science and Technology (Wrocław Tech) in 2021. He is currently a PhD student and does the research in the Department of Cybernetics and Robotics of the Wrocław Tech. His research interests include control theory for nonlinear objects, cascade control systems, and space robotics.